Journal of Ceramic Processing Research. Vol. 17, No. 7, pp. 773~777 (2016)

J O U R N A L O F
Ceramic Processing Research

Microstructural analysis of mass transport phenomena in a PEM fuel cell cathode

Seoung-Ju Lee[b], Jung Hun Yoo[a], Kwang Bo Shim[c] and Sung-Cul Yi[a,b,*]

[a]*Division of Chemical Engineering, Hanyang University, Haengdang-dong, Seongdong-gu, Seoul 133-791, Korea*
[b]*Department of Hydrogen and Fuel Cell Technology, Hanyang University, Haengdang-dong, Seongdong-gu, Seoul 133-791, Korea,*
[c]*Division of Advanced Materials Science and Engineering, Hanyang University, Haengdang-dong, Seongdong-gu, Seoul 133-791, Korea*

In a proton exchange membrane fuel cell (PEMFC), the microstructure of cathode catalyst layer (CL) is critical in the performance optimization due to the sluggish oxygen reduction reaction. Nevertheless, in most of macroscale computational fluid dynamics (CFD) model, the CL has been treated as an interface or considered to be homogeneous. The CLs are composed of four phases: carbon, ionomer, binding platinum (Pt) nanoparticles and pores. One of the most important- and most difficult-factors to model in a PEMFC is the mass transport through CLs due to the complex interconnection of the phases. To describe the phenomena in the porous CLs, the macroscopic fuel cell models employ effective transport properties for reactant and charge transport, which are exceedingly difficult to measure. In this work, the CL was characterized by the focused ion beam (FIB)-scanning electron microscope (SEM); the segmented images were integrated to create the three-dimensionally reconstructed CL for the analysis of the microstructure. The structural parameters obtained from the reconstruction were implemented into a PEMFC cathode model to investigate their influence on the prediction of cell performance. In the predicted cell polarization, the reconstruction-based parameters resulted in maximum difference of 26% in the current density at 0.7 V. Consequently, it could be argued that the reconstruction method is essential for the modeling and design of the CLs to consider the realistic microstructure.

Key words: PEMFC, Catalyst layer, Reconstruction, Model.

Introduction

The proton exchange membrane fuel cell (PEMFC) is a clean and high-efficient energy conversion device, regarded as a one of the promising power sources in the upcoming hydrogen (H_2) era [1]. The catalyst layer (CL) is the heart of PEMFC in dominating the cell performance, which must be operated over a wide range of current density. In the CLs, the hydrogen and oxygen electrochemically react to produce electricity, giving off water and waste heat. Therefore, the transport phenomena in the micro porous CL (e.g. mass or charge transport) are important for designing the PEMFCs. Gottesfeld and Zawodzinski [2], Eikerling and co-workers [3, 4] presented well-organized overviews of the CL structure and functions.

A number of model-based approaches have been conducted in the attempt to optimize the CL of PEMFC. Without consideration on the real microstructures of CL, the CL was treated either as an interface or a homogeneous porous layer in most of the PEMFC models reported in the literature [5-7]. Although the CL models based on the volume averaging approach - such as homogeneous model and agglomerate model - included the effects of CL's physical structure [8, 9], they used the structural and transport parameters based on the effective-medium approximation, which ignores the microstructural morphology and the local phenomena at the pore-level. To address this issue, Pisani et al. developed a one dimensional (1-D) analytical pore-scale model and evaluated the effects of CL pore structure on the polarization in the PEMFC by comparing the homogeneous and nonhomogeneous models [11]. Subsequently, with the reconstruction method for three-dimensional (3-D) porous structures, Mukherjee and Wang implemented direct numerical simulation (DNS) to predict the species and charge transport in the cathode CL of PEMFC [12]. However, the 3-D reconstructed structure using a stochastic generation method is still insufficient to reflect the actual microstructure of CL because it is randomly built by statistical data taken from transmission electron microscopy (TEM) measurement [13, 14].

In this work, a cathode CL in PEMFC was three-dimensionally reconstructed by using the FIB-SEM tomography. From this approach, we obtained several pore-structural parameters, including porosity, tortuosity and effective diffusivities. In addition, the structural parameters were examined in a PEMFC cathode model to highlight their importance in the CL modeling

FIB-SEM Reconstruction

The conventional cathode CL for PEMFC was

*Corresponding author:
Tel : +82-2-2220-0481
Fax: +82-2-2298-5147
E-mail: scyi@hanyang.ac.kr

prepared by using 20 wt.% Pt/C catalyst (HiSPEC 3000, Alfa Aesar) and 5 wt.% Nafion (DE512, Ion Power). As presented in Fig. 1, it was then analyzed by the FIB (Helios NanoLab 600, FEI Inc.) and SEM (JSM-6300, Jeol Inc.) for the 3-D reconstruction. The FIB Ga-ion milling was performed at 30 kV with a cutting distance of 15 nm, while SEM measurement was carried out to obtain a stack (67 slices) of images with a resolution of 1.5 × 1.5 nm. To correct the angle error of the measurements, the captured images were transformed geometrically and rearranged to into a continuous stack. Subsequently, the stack was cropped to a volume of 1 × 1 × 1 μm by the manual segmentation method for reasonable predictions [14]; the segmented images were assembled to create the 3-D reconstructed structure of the CL.

Formulation of the Model

Descriptions of the system and model assumptions

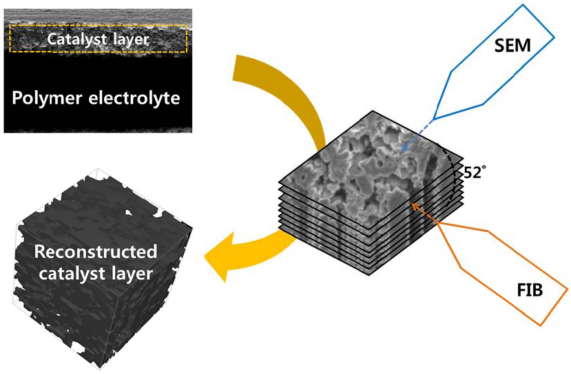

Fig. 1. 3-D reconstruction of the CL by FIB-SEM.

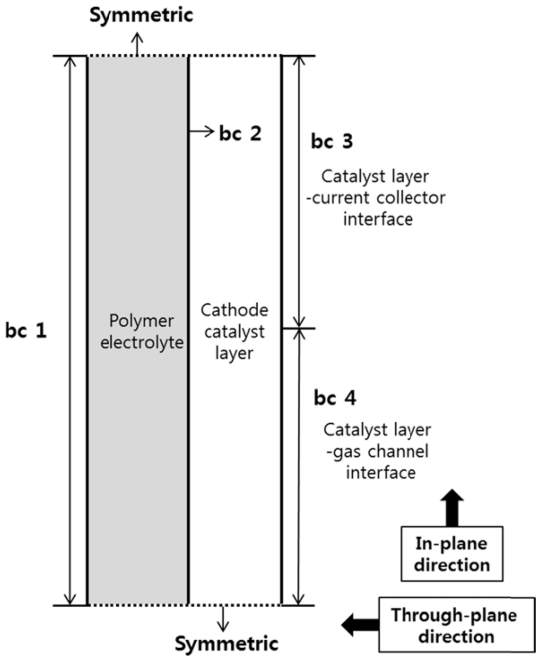

Fig. 2. A schematic of the cross-sectional domain for computational calculation.

Fig. 2 shows a cross-sectional 2-D domain of PEMFC used in this study. The symmetric domain consists of two layers: a polymer electrolyte layer (Nafion) and a cathode CL. The CL is in contact with a bipolar plate, which has current collector (bc3), and gas channel (bc4). In the CL, the cathodic reaction is as follow:

$$O_2 + 4H^+ + 4e^- \rightarrow 2H_2O \tag{1}$$

The major assumptions made to formulate the PEMFC model are listed below:

i) Steady-state operation;
ii) Isothermal conditions;
iii) Ideal gas mixture;
iv) Negligible anode overpotential;
v) Solid- and electrolyte-phase potentials that are used to describe electron and proton transport, respectively.

Governing equations

Momentum transport in the CL

In porous media, the velocity field can be evaluated by coupling Darcy's law and the mass conservation equation.

$$u = -\frac{\kappa}{\mu}\nabla p \tag{2}$$

$$\nabla \cdot (\rho u) = S_m \tag{3}$$

where κ is the permeability; and μ is the dynamic viscosity. The source term, S_m, represents the total mass change rate due to the electrochemical reactions. Thus, it is the sum of consumption/production rate of each species as follow:

$$S_m = S_{O_2} + S_{H_2O} \quad \left(S_{O_2} = -\frac{j}{4F} M_{O_2}; S_{H_2O} = \frac{j}{4F} M_{H_2O} \right) \tag{4}$$

where j, M, and F are the amount of charge generation, the molecular weight, and the Faraday constant, respectively.

Species transport in the CL

The transport of multi species, including O_2, N_2 and H_2O, occurs within the porous CL, as they are consumed or produced by the electrochemical reactions at active sites of CL. To describe the species transport, the governing equation is defined using the Maxwell-Stefan diffusion model:

$$\nabla \cdot \left(-\rho w_i \sum_m D_{i,m}^{eff} \left(\nabla x_m + \frac{1}{p}(x_m - w_m)\nabla p \right) \right) + \nabla \cdot (\rho u w_i) = S_i \tag{5}$$

where w is the mass fraction, and x is the mole fraction; S_i is the consumption/production rate of species i. The tortuosity (τ) of CL may be assumed by the well-known Bruggeman relation:

$$\tau = \varepsilon^{-0.5} \quad (6)$$

where ε is the porosity. Accordingly, the effective binary diffusivity, $D_{i,m}^{eff}$, can be calculated as:

$$D_{i,m}^{eff} = \frac{\varepsilon}{\tau} D_{i,m} = \varepsilon^{1,5} D_{i,m} \quad (7)$$

Charge Transport in the polymer electrolyte layer and CL
The continuity of current in the CL is expressed as:

$$\nabla \cdot i_s + \nabla \cdot i_e = 0 \quad (j = \nabla \cdot i_s = -\nabla \cdot i_e) \quad (8)$$

where i_s is the electronic current density in solid-phase, and i_e is the ionic current density in electrolyte-phase. The potential equations for both solid- and electrolyte-phases are obtained from Ohm's law:

$$\nabla \cdot (-\sigma_s \nabla \phi_s) = \nabla \cdot i_s \quad (9)$$

$$\nabla \cdot (-\sigma_e \nabla \phi_e) = \nabla \cdot i_e \quad (10)$$

where ϕ is the phase potential; σ is the effective electric or ionic conductivity. The amount of charge generation is given by the Butler-Volmer equation as:

$$j = A_v i_0 \left(exp\left(\frac{a_a F}{RT}\eta\right) - \frac{C_{O2}}{C_{O2\_ref}} exp\left(\frac{-a_c F}{RT}\eta\right)\right) \quad (11)$$

$$\eta = -\phi_s - \phi_e - V_{oc} \quad (12)$$

$$V_{ac} = 1.23 - 0.90 \times 10^{-3}(T - 298) \quad (13)$$

where A_v is the active area per volume; i_0, η, and V_{oc} is the exchange current density, the overpotential, and the open circuit voltage, respectively.

Numerical procedure

To solve the governing equations, the finite element-based commercial software package, COMSOL Multiphysics 5.2, was used. The boundary conditions for each equation are specified in Table 1. The stationary nonlinear solver was chosen to avoid the convergence problem. In addition, to reduce the convergence time, previous case solutions were used as initial values.

Results and Discussion

In the 3-D reconstructed CL, the effective diffusivity was estimated by the Bosanquet approximation as follow:

$$D_{i,m}^{eff} = \frac{\varepsilon}{\tau}\left(\frac{1}{D_{i,m}} + \frac{1}{D_{K,i}}\right)^{-1} \quad (14)$$

Table 1. Boundary conditions for species, momentum, electrode and electrolyte potentials.

	Momentum	Species *i*	Electrode potential	Electrolyte potential
bc 1	–	–	–	0
bc 2	Non-flux	Non-flux	Non-flux	-
bc 3	Non-flux	Non-flux	V_{cell}	Non-flux
bc 4	u_{in}	w_{i_in}	Non-flux	Non-flux

Table 2. Comparison between the assumed and reconstruction-based parameters at 353 K.

	Values based on Eq. (7)	Values obtained from the reconstruction
Porosity, ε	0.50	0.50
Tortuosity, τ	1.41	1.82
Knudsen diffusivity, $D_{K,O2}$ ($m^2\ s^{-1}$)	–	9.61e-6
Knudsen diffusivity, $D_{K,N2}$ ($m^2\ s^{-1}$)	–	1.03e-5
Knudsen diffusivity, $D_{K,H2O}$ ($m^2\ s^{-1}$)	–	1.28e-5
Effective diffusivity, $D^{eff}_{O_2,N_2}$ ($m^2\ s^{-1}$)	9.57e-6	2.07e-6
Effective diffusivity, $D^{eff}_{O_2,H_2O}$ ($m^2\ s^{-1}$)	1.22e-5	2.17e-6
Effective diffusivity, $D^{eff}_{N_2,H_2O}$ ($m^2\ s^{-1}$)	1.22e-5	2.29e-6

Table 3. Operating conditions and parameters used in the numerical model.

	Values
Operating temperature, T (K)	353
Operating pressure , p (atm)	1.0
Air-inlet mass fraction, $^{w}H_2O\_in$, $^{w}O2\_in$, $^{w}N2\_in$	0.36,0.15,0.49
Air-inlet velocity, u_{in} (m s^{-1})	3.4e-4
Ionic conductivity, σ_{el} (S m^{-1})	5.0
electronic conductivity, σ_s (S m^{-1})	1.0e3
Length of bc3 (m)	7.5e-4
Length of bc4 (m)	7.5e-4
Thickness of polymer electrolyte layer (m)	7.5e-5
Thickness of cathode catalyst layer (m)	7.5e-5
Permeability, κ (m^2)	1.0e-13
Exchange current density, i_0 (A m^{-2})	1.0e-3
Active area per volume, A_v (m^{-1})	1.0e9
Reference molar concentration, CO_{2_ref} (mol m^{-3})	3.66
Anodic and cathodic charge transfer coefficients, α_a, α_c	0.50, 0.50

$$D_{K,i} = \frac{1}{3} d_p \sqrt{\frac{8RT}{\pi M_i}} \quad (15)$$

In contrast to the effective diffusivity in Eq. (7), that in Eq. (14) strongly depends on the microstructure of the CL. For example, the pore diameter, d_p, is one of factors determining Knudsen diffusion coefficient (D_K) in Eq. (15). In addition, as shown in Table 2, the value of tortuosity is different for each equation; therefore, the effective diffusivities obtained from the reconstruction are 5-6 fold lower than that in Eq. (7).

For detailed comparison, the diffusivities that based on the Bruggeman correlation (case 1) and the 3-D reconstruction of the CL (case 2) were examined by implementing these values into the PEMFC cathode model. The operating conditions and parameters for the simulations are listed in Table 3. Fig. 3 shows the cell polarizations upon the diffusivities in the two cases. As expected, in the low current density region, the difference in the cell performance between the two cases was insignificant due the small mass transport resistance. On the contrary, the difference between the two cases was getting pronounced as the current density was increased; in particular, the relative difference was increased to 26% at 0.7 V. When the computational

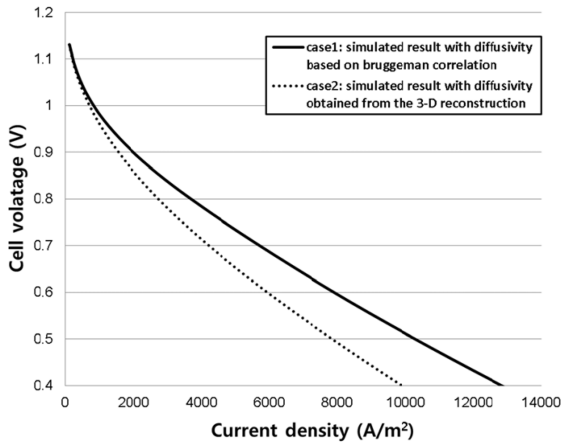

Fig. 3. Cell polarization upon the effective diffusivities.

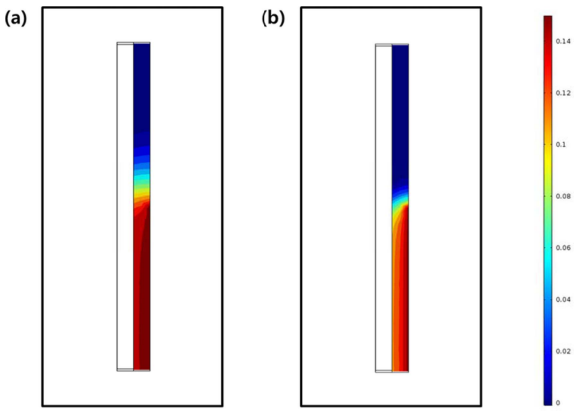

Fig. 4. Distribution of oxygen mass fraction at 0.4 V: (a) case 1, (b) case 2.

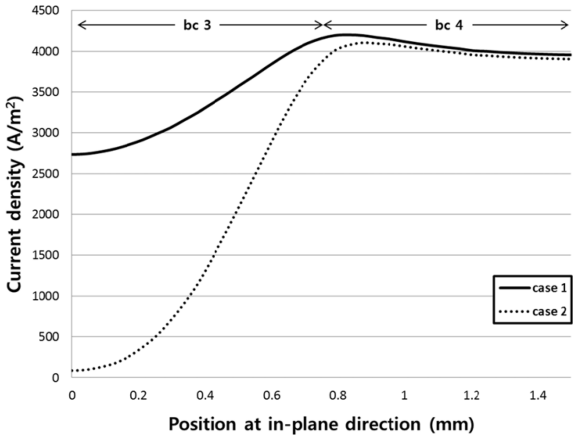

Fig. 5. Current density at 0.8 V along the in-plane direction.

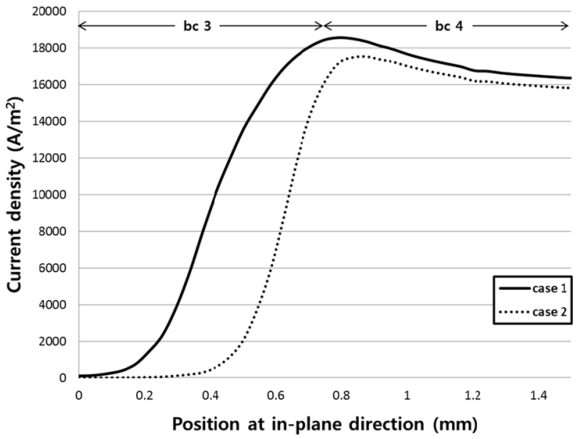

Fig. 6. Current density at 0.4 V along the in-plane direction.

domain in Fig. 2 is considered, it seems that the increased difference was due to the diffusion in in-plane direction, rather than the diffusion in through-plane direction.

To further discuss the difference between the two cases, the distribution of reactant (O_2 mass fraction) was analyzed at 0.4 V. As shown in Fig. 4, for the case 1, the reactant depletion was more severe in in-plane direction due to the longer diffusion distance. Furthermore, while the case 2 had a lager gradient of O_2 mass fraction in in-plane direction, the O_2 gradient was also noticeable in through-plane direction. Therefore, it could be said that the parameters obtained from the reconstruction are necessary for more realistic projection of the reactant diffusion in both of the two directions.

On the other hand, Figs. 5 and 6 show the current density along the in-plane direction at 0.8 V and 0.4 V, respectively. Under the air-inlet (bc4) in Fig. 5, the difference in current densities between the two cases was less than 2.0%, except near the current collector (bc3). However, the difference was more than 95%, as the current density of case 2 was rapidly declined along the in-plane direction. In Fig. 6, the gap between the two cases was approximately 4% under the bc4, and it was increased to 98% at the end of position. This point can be explained by the reactant distribution in Fig. 4 which

determines the electrochemical reaction rate. Consequently, to avoid overestimation of the cell performance and to minimize uncertainty in the prediction, the microstructural parameters based on the 3-D reconstruction should be considered in the macroscale model.

Conclusions

In this study, the microstructural parameters and effective diffusivities were obtained from the 3-D reconstruction of the CL by FIB-SEM measurement. Subsequently, these values were implemented into a PEMFC cathode model to compare their results with that of the assumed effective diffusivity based on the Bruggeman correlation. In the predicted cell polarization, the maximum difference between the two cases (case1: Bruggeman correlation-based, case 2: the reconstruction-based) was 26% at 0.7 V. In addition, the reactant distribution in the two cases revealed that the parameters obtained from the reconstruction had a non-negligible impact on the diffusion in both the in-plane and the through-plane directions at the high current density. This observation was confirmed again by the analysis of current density distributions along the in-plane direction for the two cases. From our results, it is obvious that the reconstruction-based parameters are essential for the modeling and design of CLs as these reflect the effects of realistic microstructure on mass transport.

Acknowledgments

This research was supported by the Ministry of Trade, Industry & Energy (MOTIE), Korea Institute for Advancement of Technology (KIAT) through the Encouragement Program for the Industries of Economic Cooperation Region.

Nomenclature

A_v	Active surface area per unit volume (m^2 m^{-3})
C	Molar concentration (mol m^{-3})
d_p	Pore diameter (m)
D	Diffusion coefficient (m^2 s^{-1})
F	Faraday constant (96485 C mol^{-1})
i	Current density (A m^{-2})
i_0	Exchange current density (A m^{-2})
j	Amount of charge generation (A m^{-3})
M	Molecular weight (kg mol^{-1})
R	Universal gas constant (8.314 J mol^{-1} K^{-1})
p	Pressure (atm)
S	Source term (kg m^{-3} s^{-1})
T	Temperature (K)
u	Velocity (m s^{-1})
V_{cell}	Cell voltage (V)
V_{oc}	Open circuit voltage (V)
w	Mass fraction
x	Mole fraction

Greek letters

α	Charge transfer coefficient
ε	Porosity
η	Over potential (V)
κ	Permeability (m^2)
μ	Dynamic viscosity (Pa s)
ρ	Density (kg m^{-3})
σ	Charge conductivity (S m^{-1})
τ	Tortuosity
ϕ	Phase potential (V)

Subscripts & superscripts

a	Anodic
c	Cathodic
e	Electrolyte phase
eff	Effective
i	Species
in	Inlet
K	Knudsen diffusion
m	Species or mass
ref	Reference
s	Solid phase

References

1. B.C.H. Steele and A. Heinzel, Nature 414 (2001) 345-352.
2. S. Gottesfeld and T.A. Zawodzinski, Advances in Electrochemical Science and Engineering 5 (1997) Wiley and Sons, New York p. 226.
3. M. Eikerling, A.A. Kornyshev, and A.A. Kulikovsky, Encyclopedia of Electrochemistry (2007) Wiley-VCH, Weinheim p. 125.
4. M. Eikerling, A.A. Kornyshev, and A.A. Kulikovsky, Fuel Cell Rev. January (2005) 24.
5. T. Berning and N. Djilali, J. Electrochem. Soc. 150 (2003) A1589-A1598.
6. U. Pasaogullari and C.Y. Wang, J. Electrochem. Soc. 152 (2005) A380-A390.
7. D.M. Bernardi and M.W. Verbrugge, AIChE J. 37 (1991) 1151-1163.
8. C.Y. Wang, Chem. Rev. 104 (2004) 4727-4766.
9. A.Z. Weber and J. Newman, Chem. Rev. 104 (2004) 4679-4726.
10. M. Sahimi, Application of Percolation Theory (1994) Taylor & Francis, Bristol, PA p. 126.
11. L. Pisani, M. Valentini, and G. Murgia, J. Electrochem. Soc. 150 (2003) A1558-A1568.
12. P.P. Mukherjee and C.Y. Wang, J. Electrochem. Soc. 154 (2007) B1121-B1131.
13. P.P. Mukherjee, C.Y. Wang and Q. Kang, Electrochim. Acta 54 (2009) 6861-6875.
14. S. Thiele, T. Furstenhaupt, D. Banham, T. Hutzenlaub, V. Birss, C. Ziegler, and R. Zengerle, J. Power Sources 228 (2013) 185-192.